Title

Multimodal Assessment of Microscopic Morphology and Retinal Function in Patients With Geographic Atrophy

Journal

Investigative Ophthalmology & Visual Science, 54(6)

ISSN

0146-0404

Authors

Panorgias, Athanasios
Zawadzki, Robert J
Capps, Arlie G
et al.

Publication Date

2013-06-25

DOI

10.1167/iovs.12-11525

Peer reviewed

Multimodal Assessment of Microscopic Morphology and Retinal Function in Patients With Geographic Atrophy

Athanasios Panorgias,[1] Robert J. Zawadzki,[1,2] Arlie G. Capps,[1,3,4] Allan A. Hunter,[1] Lawrence S. Morse,[1] and John S. Werner[1,5]

[1]Department of Ophthalmology and Vision Science, University of California, Davis, Davis, California
[2]Department of Cell Biology and Human Anatomy, University of California, Davis, Davis, California
[3]Institute for Data Analysis and Visualization, Department of Computer Science, University of California, Davis, Davis, California
[4]Lawrence Livermore National Laboratory, Livermore, California
[5]Department of Neurobiology, Physiology and Behavior, University of California, Davis, Davis, California

Correspondence: Athanasios Panorgias, Department of Ophthalmology and Vision Science, School of Medicine, University of California, Davis, 4860 Y Street, Suite 2400, Davis, CA 95817;
apanorgias@ucdavis.edu.

Submitted: December 19, 2012
Accepted: May 12, 2013

Citation: Panorgias A, Zawadzki RJ, Capps AG, Hunter AA, Morse LS, Werner JS. Multimodal assessment of microscopic morphology and retinal function in patients with geographic atrophy. *Invest Ophthalmol Vis Sci*. 2013;54:4372–4384.
DOI:10.1167/iovs.12-11525

Purpose. To correlate retinal function and visual sensitivity with retinal morphology revealed by ultrahigh-resolution imaging with adaptive optics–optical coherence tomography (AO-OCT), on patients with geographic atrophy.

Methods. Five eyes from five subjects were tested (four with geographic atrophy [66.3 ± 6.4 years, mean ± 1 SD] and one normal [61 years]). Photopic and scotopic multifocal electroretinograms (mfERGs) were recorded. Visual fields were assessed with microperimetry (mP) combined with a scanning laser ophthalmoscope for high-resolution confocal retinal fundus imaging. The eye tracker of the microperimeter identified the preferred retinal locus that was then used as a reference for precise targeting of areas for advanced retinal imaging. Images were obtained with purpose-built, in-house, ultrahigh resolution AO-OCT. Fundus autofluorescence (FAF) and color fundus (CF) photographs were also acquired.

Results. The AO-OCT imaging provided detailed cross-sectional structural representation of the retina. Up to 12 retinal layers were identified in the normal subject while many severe retinal abnormalities (i.e., calcified drusen, drusenoid pigment epithelium detachment, outer retinal tubulation) were identified in the retinae of the GA patients. The functional tests showed preservation of sensitivities, although somewhat compromised, at the border of the GA.

Conclusions. The images provided here advance our knowledge of the morphology of retinal layers in GA patients. While there was a strong correlation between altered retinal structure and reduction in visual function, there were a number of examples in which the photoreceptor inner/outer segment (IS/OS) junctions lost reflectivity at the margins of GA, while visual function was still demonstrated. This was shown to be due to changes in photoreceptor orientation near the GA border.

Keywords: geographic atrophy, adaptive-optics OCT, multifocal ERG, scotopic mfERG, microperimetry

Late stage AMD may have two different phenotypes, the neovascular and the atrophic. The result of advanced atrophic AMD is geographic atrophy (GA), which is defined as a sharply demarcated round/oval area of hypopigmentation with corresponding visual field scotomas or reduced sensitivities.[1] The size criteria of the geographic hypopigmentation has been somewhat debated (200 μm or greater), but the clinical prognostic significance of the loss of a large confluent area of RPE (and outer neurosensory retina), especially if it involves the fovea, must be emphasized. Approximately 85% to 90% of AMD patients will develop an atrophic area,[2] where the photoreceptor layer and the RPE deteriorate and finally necrose.[1,3] The pathophysiology of the disease still remains unclear and many factors are postulated to affect the onset of GA, including oxidative damage, toxic compound accumulation in the RPE lysosomes, inflammatory processes, nonregulated complement system, and neurodegeneration,[4,5] all of which are associated with dietary, environmental, and genetic risk factors.[6,7] Therefore, the therapeutic challenges of advanced atrophic AMD are great and new options to slow vision loss are being pursued.[8]

Optical coherence tomography (OCT) and fundus autofluorescence (FAF) are two imaging modalities that offer valuable information about the structure of atrophic lesions.[9–13] Because FAF and spectral domain OCT (SD-OCT) are becoming standard clinical imaging modalities, their use may facilitate understanding of the clinical disease phenotype in determining AMD progression. On an FAF image, the GA areas appear hypoautofluorescent due to the absence of lipofuscin, otherwise present in the RPE lysosomal compartment.[14] SD-OCT studies demonstrate that the areas around the atrophy show evidence of anatomical changes, the severity of which is linked to disease progression.[10,13,15] RPE cells have been found to have an irregular shape and lose their structural organization, while photoreceptors become less distinguishable closer to the lesion.[10] Photoreceptor layer loss was found to progress even

TABLE. Subjects' Demographics

Subject	Sex	Age	BCVA		Refraction, D		AMD Type		History of Anti-VEGF Therapy		Fixation
			Tested Eye	Fellow Eye	Tested Eye	Fellow Eye	Tested Eye	Fellow Eye	Tested Eye	Fellow Eye	
N1	M	61	20/20-1	20/16-2	0	−1.50	N/A	N/A	N/A	N/A	Central
GA1	F	62	20/60	20/20-2	0.75	0.75	Atrophic AMD	Atrophic AMD	NO	NO	Central
GA2	M	74	20/25-2	20/25-2	−1.25	−1.00	Atrophic AMD	Atrophic AMD	NO	NO	Central
GA3	F	60	20/50	20/70	−1.00	−1.00	Atrophic AMD	Neovascular AMD	NO	NO	Central
GA4	F	69	20/200	CF @ 1′	1.00	−1.00	Atrophic AMD	Disciform scar	Yes (last on 08/2010)	NO	Eccentric

D, diopters.

outside the margins of atrophy where RPE is still present, although likely dysfunctional.[9] SD-OCT is invaluable for detecting and monitoring retinopathies; and when it is combined with adaptive optics (AO), it offers unprecedented lateral resolution so that single photoreceptor cells and microcapillaries may be resolved.[16] Due to the still relative novelty of the AO instruments and lack of commercial availability, AO-OCT systems haven't been used extensively for patient imaging, with a few exceptions.[16–23]

There are certain caveats, though, in the interpretation of GA lesions using FAF and SD-OCT. For example, in an FAF image, drusen may appear hypoautofluorescent and therefore cannot be differentiated from atrophy.[24] This results in a false interpretation, as the still functioning drusenoid areas are miscategorized as atrophic lesions. Additionally, the areas with RPE loss on an SD-OCT scan show deeper penetration of the OCT beam into the choroid. However, this is not observed in cases where overlying structures (i.e., calcified drusen) block the OCT light from penetrating deeper in retinal structures. It is also important to note that retinal imaging—such as FAF and SD-OCT—lacks functional information, which is very important for following the progression of GA or, for example, in the identification of drusen versus atrophic lesions.[24] Therefore, high spatial resolution functional testing combined with detailed structural imaging is essential for diagnostic and disease monitoring.

Two of the main functional tests in ophthalmology clinics are ERG and perimetry. ERGs measure the responses of outer or inner retinal cells to light stimulation and are widely used to diagnose and monitor retinal abnormalities.[25–27] In multifocal ERGs (mfERG), which offer an objective probe of spatially resolved retinal responses,[28] electrical responses are recorded simultaneously from many small retinal patches being simultaneously exposed to a flickering hexagonal pattern. mfERGs have been used extensively for early detection and monitoring of AMD where N1 and P1 amplitudes are decreased and N1 latency is delayed.[29–31] Although histopathological and some psychophysical studies show that the rod-mediated system is more vulnerable than the cone-mediated system, results from scotopic full-field ERGs (ffERGs) and mfERGs studies are conflicting.[32,33] Jackson et al.[34,35] showed that scotopic ffERG a- and b-wave responses are different from normal only in late and not early stage AMD while scotopic mfERGs showed impairment in eyes with early age-related maculopathies.[36–38] Because of the spatial information about retinal function the mfERG contains, it can be compared with other structural and functional modalities such as fundus imaging and mP.[39–43] The latter proved to be a valuable functional test especially with older subjects with diseased eyes having low visual acuity and consequently poor fixation. It tests the sensitivity in the macular area while simultaneously tracking the retinal fundus, allowing the detection and precise localization of any retinal abnormalities. Almost a one-to-one correspondence between increased FAF and reduced light sensitivity, as measured with mP, has been shown in studies of early AMD patients.[44] Other studies have shown that sensitivity reduction is not specific to the drusen or atrophic area but rather spreads to adjacent areas, implying that retinal function is compromised even in areas without any observable morphological changes.[45,46] As with structural imaging, there are several factors that limit the spatial resolution of the mfERG and mP testing. The limiting factors in mfERGs are the recording time and the signal-to-noise ratio. An increase in the number of hexagons requires either an increase in the testing time or a loss in the signal-to-noise ratio, leading to patient fatigue and possibly loss of test reliability, respectively. In microperimetry, test time is also a limiting factor. Increasing the number of testing points increases testing time, making the task tiring and less reliable, especially with subjects having poor vision and fixation. However, both tests offer the best spatial resolution among functional clinical tests available to date.

As the progression and pathophysiology of GA are not yet well understood, a combination of the structural and functional imaging modalities may offer new insights in understanding the disease. In this paper, we demonstrate the utility of probing GA with both functional and structural modalities in a small number of patients who were tested extensively with both commercial and purpose-built instruments. We show good agreement between structure and function in most cases, but there may be apparent exceptions unless photoreceptor orientation can be visualized.

METHODS

Subjects

Five subjects (see Table) were recruited from the UC Davis Eye Center. Four subjects had unilateral or bilateral AMD and one was normal. Written informed consent was obtained after explanation of the nature and possible consequences of the study. This research followed the tenets of the Declaration of Helsinki and was approved by the University of California, Davis' Institutional Review Board. The subjects completed a battery of tests (mP, photopic and scotopic mfERGs, AO-OCT) during two to three lab visits. CF images of 50° without any filters were obtained with a retinal camera (TRC.501X Mydriatic Retinal Camera; Topcon Medical Systems, Inc., Tokyo, Japan). FAF images of 30° were obtained with a commercial OCT device (SPECTRALIS HRA+OCT; Heidelberg Engineering, Heidelberg, Germany) with excitation at 488 nm and emission $>$ 500 nm, following standard clinical protocol. To increase signal-to-noise ratio the FAF device (Heidelberg Engineering) is equipped with an eye tracker and averages multiple FAF frames.

All of the GA subjects had fluorescein angiography (FA) verifying the absence of active fluorescein leakage prior to study enrollment. GA subjects 1 through 3 had extensive

clinical examinations (stereoscopic fundoscopic examination, FA, macula OCT) without any history of conversion to/from neovascular AMD. GA subjects 1 through 3 have never received any treatments for exudative disease (e.g., anti-VEGF, laser treatment, etc.). GA subject 4 had a history of neovascular AMD in the study eye that was treated with four ranibizumab injections last April 2007, and was continued on "maintenance injections" of bevacizumab until the last injection in August 2010. Areas of subretinal fibrosis of the inferior juxtafoveal macula correspond to the occult areas of leakage noted in original FAs when ranibizumab injections were given. Since the last ranibizumab injection of early 2007, clinical exams, FAs, and OCTs have failed to show recurrence of fluid.

Microperimetry

A commercial microperimeter (MAIA; CenterVue, Padova, Italy) was used to assess light sensitivity. A grid of 68 stimuli (Goldman III), covering the central 20° of visual field, was used. The distance between two stimuli was approximately 2.2°. The MAIA uses a line scanning-laser ophthalmoscope (SLO) for fundus tracking and identification of the preferred retinal locus (PRL). Prior to the beginning of data acquisition, training was given to the subject to familiarize him/herself with the procedure and the equipment in a room with dimmed lights for approximately 10 minutes. The subjects were instructed to fixate on a small central red circle and press a handheld button every time a stimulus was seen anywhere in their visual field. Once a satisfactory fundus image was obtained with the SLO, the operator identified the center of the optic disk on the image and then the testing began. The microperimeter (MAIA; CenterVue) projected 10 stimuli on the optic disk during testing to ensure fundus tracking was successful. The fundus image obtained with the SLO was used for image registration with other modalities.

Multi-Focal Electroretinograms

Photopic and scotopic mfERGs were recorded from the same eye of each subject that was used for imaging. The visual response imaging system software (Veris Pro 6.3.2; EDI, Redwood City, CA) was used with the FMSIII stimulator running at 75 Hz (EDI). mfERG responses were obtained with a DTL electrode and standard ground and reference gold cup electrodes placed at the forehead and close to the temporal canthus, respectively. The pupil was maximally dilated with 1% tropicamide and 2.5% phenylephrine. A fixation target on the central hexagon was used for the subjects whose PRL coincided with the fovea. Subject GA4 had no central fixation as her fovea fell within an atrophic area. To make comparisons with normal values, the fixation target was moved so that the central hexagon was projected onto the fovea. The size of the fixation target varied among subjects for easy identification. For all cases, the target's diameter was $\leq 4°$. A blinking fixation target was employed in order to hold the subject's attention. During each segment, the fixation target blinked 3 to 10 times and the subjects were instructed to count the blinks and report the number at the end of the recording. This task is challenging even for young and healthy subjects, but it was found to be effective for maintaining alertness. An infrared camera in the FMSIII stimulator (EDI) allows a fundus image to be acquired with the hexagonal pattern superimposed. This was used for precise registration of the ERG traces with the patient's CF. Comparisons between the subjects of this experiment and age-matched normals were made using our database of normal subjects tested under identical conditions.

Photopic mfERGs. The standard scaled 103-hexagonal pattern was used to obtain the photopic mfERGs. An m-sequence of 16 was used, and required approximately 14 minutes of recording time split into segments of approximately 30 seconds. The luminance of the bright and dark states were 200 cd/m^2 (white) and near zero, respectively, to produce maximum contrast. The luminance of the background was 100 cd/m^2. The amplifier gain was 100K, and the low- and high-frequency cut off was set to 10 and 300 Hz, respectively. To better visualize the areas of atrophy no spatial averaging was used and the signal was digitally filtered offline for frequencies higher than 100 Hz.

Scotopic mfERGs. Scotopic mfERG responses were recorded after a 40-minute period of dark adaptation. An unscaled 61-hexagonal pattern was used to elicit the responses from the central ~40°, resulting in a resolution of ~4.4°. An m-sequence of 14 resulted in approximately 14 minutes recording time that was split into 30-second segments. Inserting three blank frames (one before the stimulus and two after) slowed the m-sequence. Only the blue LED of the system (peak wavelength ~450 nm) was used, to better control the spectral output of the stimulator (FMSIII stimulator; EDI).[47] A linear polarizer and a Kodak Wratten-47B filter (Kodak, Rochester, NY) were placed in front of the stimulator to produce scotopic luminances. The luminance of the bright state was −2.5 log cd/m^2 and that of the dark state close to zero resulting in more than 99% contrast. The background luminance was the mean luminance (−2.8 log cd/m^2) of the two states. The amplifier gain was 100K, and the low- and high-frequency cut off was set to 3 and 100 Hz, respectively.

Adaptive Optics–Optical Coherence Tomography

The AO-OCT system used for imaging has already been described in detail elsewhere.[48] Briefly, The AO-OCT sample arm consisted of a series of focal telescopes to image the eye's pupil on all the key optical components (vertical and horizontal scanning mirrors, wavefront corrector [high stroke 97-actuator ALPAO membrane magnetic deformable mirror (DM)]), the Hartmann-Shack wavefront sensor (WFS), and the fiber collimator with achromatizing lens used for light delivery and detection of the OCT channel). The magnification factor between the eye's pupil and the DM was ×48/25 (~13.5 mm diameter), based upon the 7.0-mm subject's pupil diameter used for imaging. The magnification between the eye and the WFS was ×36/25 (~10.1-mm diameter). This allows for <3 μm lateral resolution when diffraction-limited, AO-corrected retinal images are acquired.

The light source for OCT in the current configuration is a Superluminescent BroadLighter diode operating at 836 nm with 112-nm spectral bandwidth (Superlum Ltd., Cork, Ireland), allowing 3.5-μm measured axial resolution at the retina yielding ~3 × 3 × 3.5 μm^3 volumetric resolution. A custom achromatizing lens was developed for correction of the eye's longitudinal chromatic aberration across the near infrared wavelengths at which the broadband light source operates. The same light source was used for both wavefront sensing and AO-OCT imaging. The AO-OCT B-scans consisted of 1000 A-scans acquired with 50-μs exposure time that resulted in 18 kHz A-scan rate. A bite-bar and a forehead-rest assembly mounted on an X-Y-Z remote-controlled motorized translation stage was used to reduce head motion and allow precise positioning of the eye's pupil in the center of the imaging system's entrance pupil. A computer monitor was used to project a fixation target that was aligned with the imaging system. To ensure the maximum pupil size and minimize fluctuations in accommodation, the subject's eye was dilated and cyclopleged as before (see "mfERGs" section). Moisturizing eye drops were used to reduce corneal drying during imaging. All AO-OCT B-scans, shown in this manuscript, are

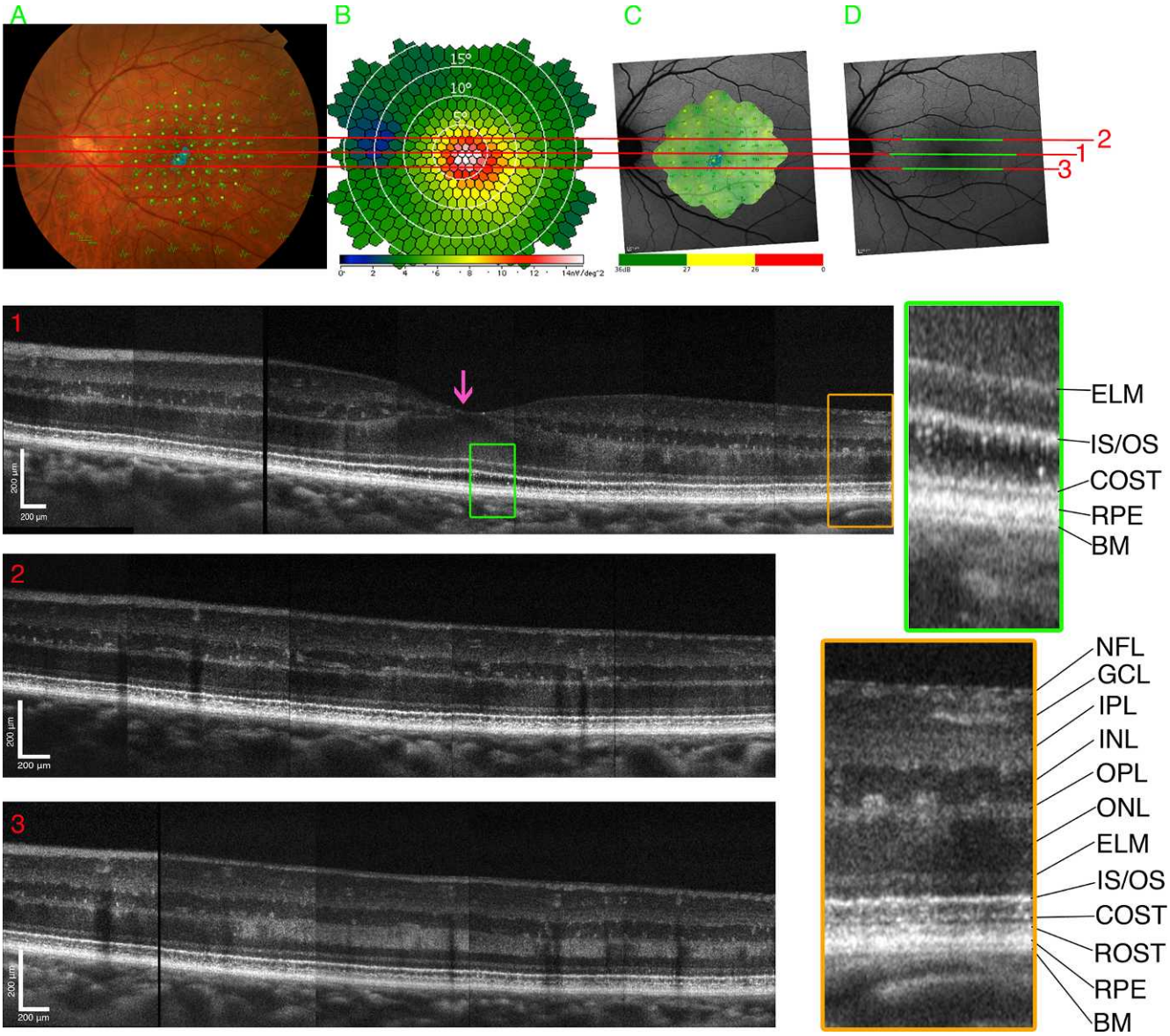

Figure 1. Results from normal subject. (**A**) CF with the photopic mfERG traces and mP sensitivity superimposed (provided also in the Supplementary Material for viewing at higher magnification). (**B**) Shows the mfERG response density map. (**C**) Shows the mP sensitivity map superimposed on the FAF. (**D**) FAF. The three *numbered green lines* in (**D**) correspond to the three B-scan montages shown below. The *magenta arrow* in B-scan 1 shows the PRL. The two areas within the *green* and *amber rectangles* correspond to the magnified B-scans shown on the *right*. BM, Bruch's membrane; RPE, retinal pigment epithelium; ROST, rod outer segment tip; COST, cone outer segment tip; IS/OS, inner segment/outer segment junction; ELM, external limiting membrane; ONL, outer nuclear layer; OPL, outer plexiform layer; INL, inner nuclear layer; IPL, inner plexiform layer; GCL, ganglion cell layer; NFL, nerve fiber layer.

intensity averages of five consecutive motion registered B-scans using a software plugin (ImageJ StackReg; Biomedical Imaging Group, Lausanne VD, Switzerland).[49,50] Large field AO-OCT B-scans were created by stitching several averaged AO-OCT B-scans together. Unavoidably, there are some gaps between the areas we imaged that are represented as black strips in the stitched B-scans.

The names of the OCT retinal layers used in this paper, specifically photoreceptor bands, take into account wave-guiding properties of photoreceptors based on their macroscopic morphology rather than recently proposed anatomical correlates.[51,52] The names of the bands are correlated with the optical structures that should create OCT signals according to the optical wave-guiding theory, namely due to changes of the wave-guiding properties between inner and outer segments[53] and back-reflection from the fiber tip (i.e., end of cone and rod outer segments, COST and ROST, respectively).[54] These names are also in agreement with the experimental observations of the Stiles-Crawford effect.[55]

Results

The same set of images (Figs. 1–5) was created for each of the five subjects (Table). Figure 1 shows the results for the normal subject. His photopic mfERG traces and mP thresholds are superimposed on the CF (Fig. 1A). Figures 1A, 2A, 3A, 4A, and 5A from all the subjects are available in the Supplementary Material for viewing at higher resolution. Figure 1B shows the photopic mfERG response density; Figure 1C shows the mP

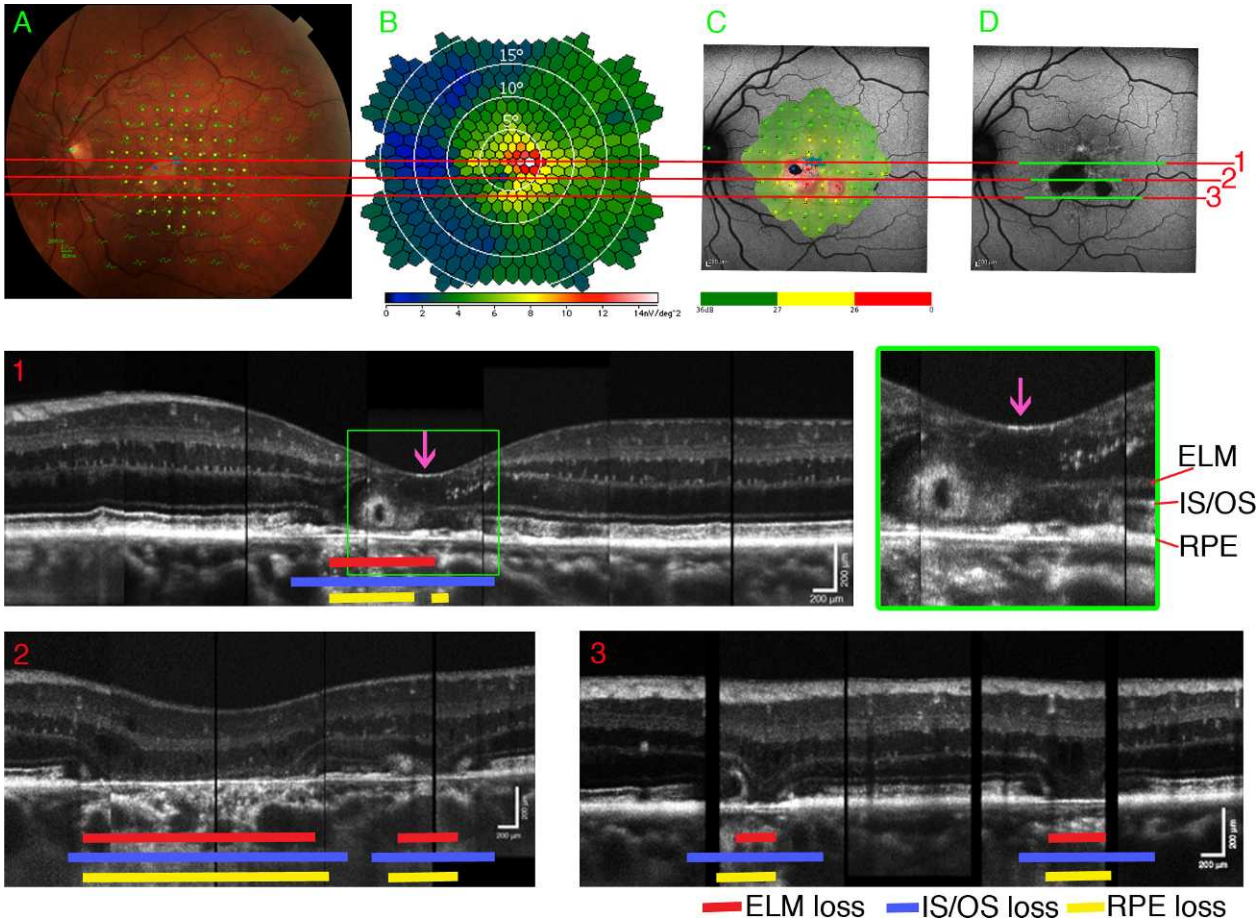

Figure 2. Results from subject GA1. The panel layout is the same as in Figure 1. The *red*, *blue*, and *yellow* bars on the B-scans correspond to ELM, IS/OS, and RPE loss, respectively. The magnified B-scan section shows remaining RPE that corresponds to the location of the PRL.

color-coded sensitivity map registered on the FAF image; and Figure 1D is the FAF alone. Figures 1A through 1D are aligned. To facilitate comparisons, the AO-OCT B-scans shown below are numbered from 1 to 3, and the numbers correspond to the three horizontal lines on the top four panels. The three green lines in Figure 1D correspond to the three B-scans. B-scan no. 1 corresponds to the central B-scan that runs through the PRL of the subject (shown by the magenta arrow). The PRL, identified by the mP, also corresponds to the central mfERG hexagon on Figures 1A and 1B. For the control subject photopic mfERGs, mP, CF, FAF, and AO-OCT B-scans show no abnormalities. The mfERG response density (Fig. 1B) peaks at the fovea corresponding to the highest cone density and falls gradually in the peripheral macula. On the left, there is an area with reduced response density (denoted by blue values) due to the optic nerve head. mP shows normal sensitivity values with the fovea being more sensitive. FAF shows no areas of hyper- or hypopigmentation and the three AO-OCT B-scans show normal retinal structure. Two retinal areas (at $\sim$1° and 9° temporally) are shown at higher magnification to make the retinal band identification easier (for detailed explanation, see Fig. 1 caption).

Subject GA1 (Fig. 2) has advanced atrophic AMD with two areas of GA and soft drusen. RPE mottling and small hard drusen are also evident. FAF shows two hypoautofluorescent atrophic areas that correspond to functional scotomas (determined by photopic mfERGs and mP) with surrounding hyperautofluorescence. Photopic mfERG traces on the atrophic locations show reduced N1- and P1-wave amplitude (response density < -2 SD from age-matched normals). However, peri-GA hexagons show partially restored function with attenuated waveforms compared with the aged-matched controls (response density between ± 1.2 SD from normal values), as shown in Figure 6. The two atrophic areas show reduced light sensitivity with mP (>8 SD from age-matched normals), but outside the atrophy sensitivity is gradually restored (less than 6 SD in the peri-GA and less than 2.09 SD in the non-GA area from age-matched normals). AO-OCT imaging correlates RPE/outer retinal atrophy with these loci of suppressed function. Figure 2, B-scan 1 shows part of the large atrophic area in the fovea and an outer retinal tubulation nasally. The red bars show the extent of external limiting membrane (ELM) loss; the yellow bars show the extent of RPE loss; and the blue bars denote the extent of inner segment/outer segment (IS/OS) junction loss. The ELM loss corresponds approximately to the RPE loss while the IS/OS junction loss is greater than both, as illustrated on an AO-OCT B-scan. The PRL (magenta arrow) falls within the central RPE atrophy, with loss of IS/OS junction reflectivity. However, the ELM extends up to the PRL, as seen in the magnified portion of this scan, and remaining RPE is evident underneath the PRL. B-scan 2 shows two atrophic regions. The left larger GA is similar to the atrophy in B-scan 1 with additional loss of the ELM and severely reduced light sensitivity, determined by mP, and almost absent ERG signal. The second smaller GA on the right side of B-scan 2, again shows loss of IS/OS reflectivity with preservation of the ELM and preserved function (mP and mfERGs) similarly to the PRL and B-scan 1. B-scan 3 shows the GA border of two

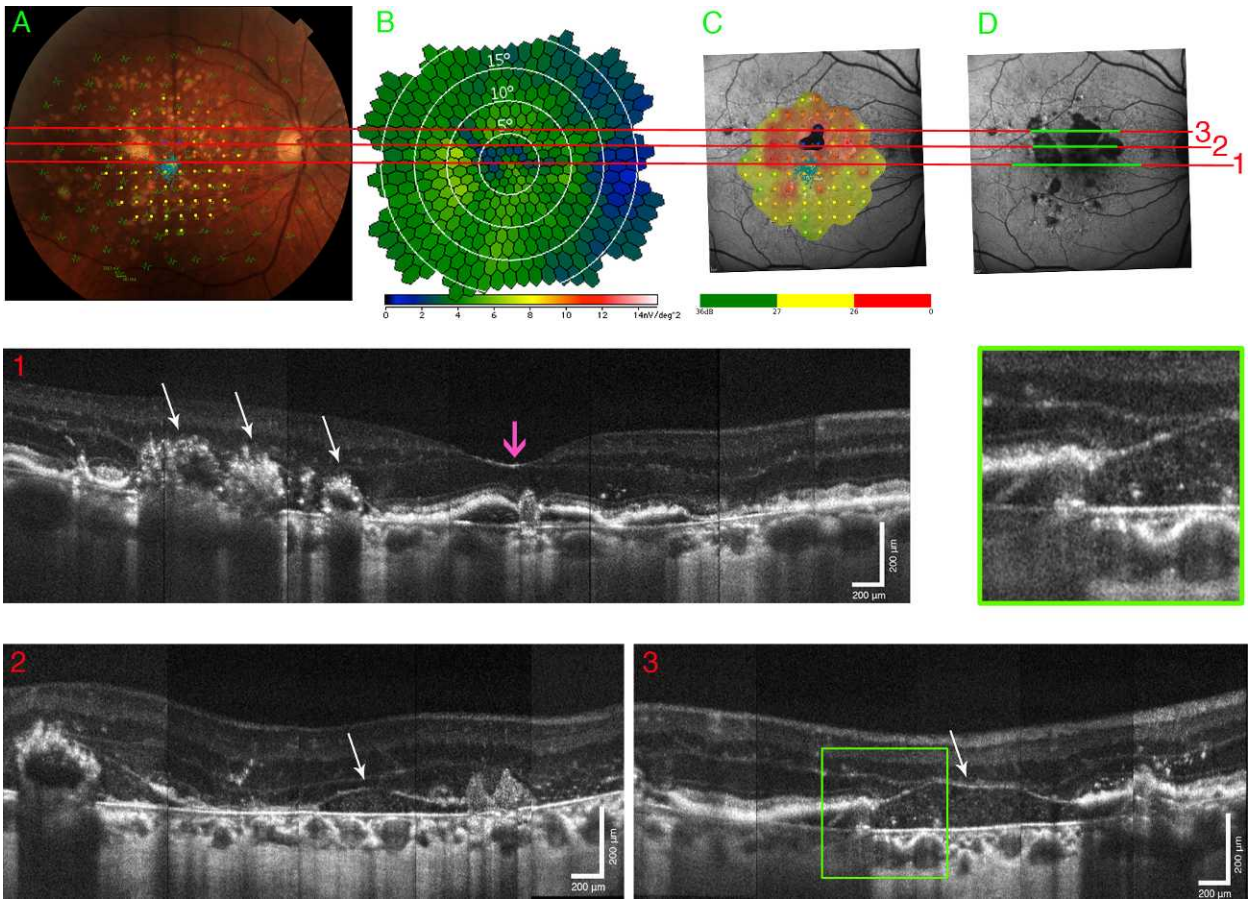

FIGURE 3. Results from subject GA2. The panel layout is the same as in Figure 1. The *white arrows* on scan 1 show the formation that corresponds to calcified drusen. The *white arrows* on scans 2 and 3 show the drusenoid PED (also shown magnified).

inferior areas of atrophy with IS/OS loss of reflectivity. The ELM appears to be partially preserved in the left GA while it is not visible in the right GA of B-scan 3. Functionality is preserved and follows the anatomical findings shown in B-scan 3.

Subject GA2 (Fig. 3) has advanced atrophic AMD. Several soft drusen and drusenoid pigment epithelial detachment (PED) in the peripheral macula are juxtaposed with calcified drusen and associated atrophy of the central macula. The FAF shows areas of atrophy with surrounding reticular autofluorescence. Photopic mfERG response density is abnormal in the central-superior macula (>3 SD from age-matched normals), but normal elsewhere. However, implicit time is delayed across the area tested (>2 SD from age-matched normals). mP results show no sensitivity in the inferior atrophic lesion and reduced sensitivity in the superior part of the macula (>4 SD from age-matched normals). The inferior macular area is more sensitive to light than the superior macula, with the exception of two spots that correspond to the two small atrophic lesions in this area. Even though sensitivity is absent or low in the atrophic lesions, there are several loci between the different atrophic areas that show some sensitivity to light. AO-OCT scans show extensive retinal damage. The central B-scan (1) shows PED and GA in several locations. There are also three formations to the left side of the B-scan that are hypoautofluorescent in FAF, but they cannot be identified as RPE atrophy (white arrows). B-scans 2 and 3 reveal a drusenoid PED progressed into geographic atrophy and corresponds to the superior-central atrophic lesion shown in FAF. The thin layer (white arrows) possibly is the interface between inner retina and drusenoid deposits. There is a complete loss of outer retina in the middle of scan 3, which corresponds to complete lack of function as measured by mfERGs and mP.

Subject GA3 (Fig. 4) has advanced GA with RPE changes. Decreased autofluorescence delineates the atrophic lesions that lack a hyperautofluorescent edge. Photopic mfERG response density is diminished in the atrophic areas (>4 SD from age-matched normals), but is restored in areas that show no hypoautofluorescence in FAF. FAF reveals areas of speckled hyperautofluorescence in temporal-superior and temporal retina; however, photopic mfERG response density is normal in the first case and abnormal in the second (>2 SD from age-matched normals). The photopic mfERG implicit time is delayed in the majority of the hexagons. mP results show complete loss of light sensitivity in two areas of hypoautofluorescence (blue-colored spots in Fig. 4C) and severely reduced light sensitivity in the surrounding areas (>5 SD from age-matched normals). Interestingly, within the nasal atrophy both photopic mfERGs and mP show an area of retinal activity (white arrows in Figs. 4B, 4C). The AO-OCT B-scans show areas of RPE atrophy with functional retinal tissue in between. It can be seen in B-scan 1 that the PRL (magenta arrow) falls at the border of the RPE atrophy and at the edge of a hyporeflective wedge-shaped band.[56] B-scan 2 shows a druse at the edge of the central atrophic area (shown also in higher magnification) with remaining RPE and ELM reflectivity on both sides but, interestingly, without reflectivity from the IS/OS junction within approximately 300 µm. The right edges of B-scans 1 and 2 show intact retinal organization that corresponds to the preserved functional retina within the nasal atrophy (white arrows on B-scans 1, 2, and panels B and C). Finally, FAF shows

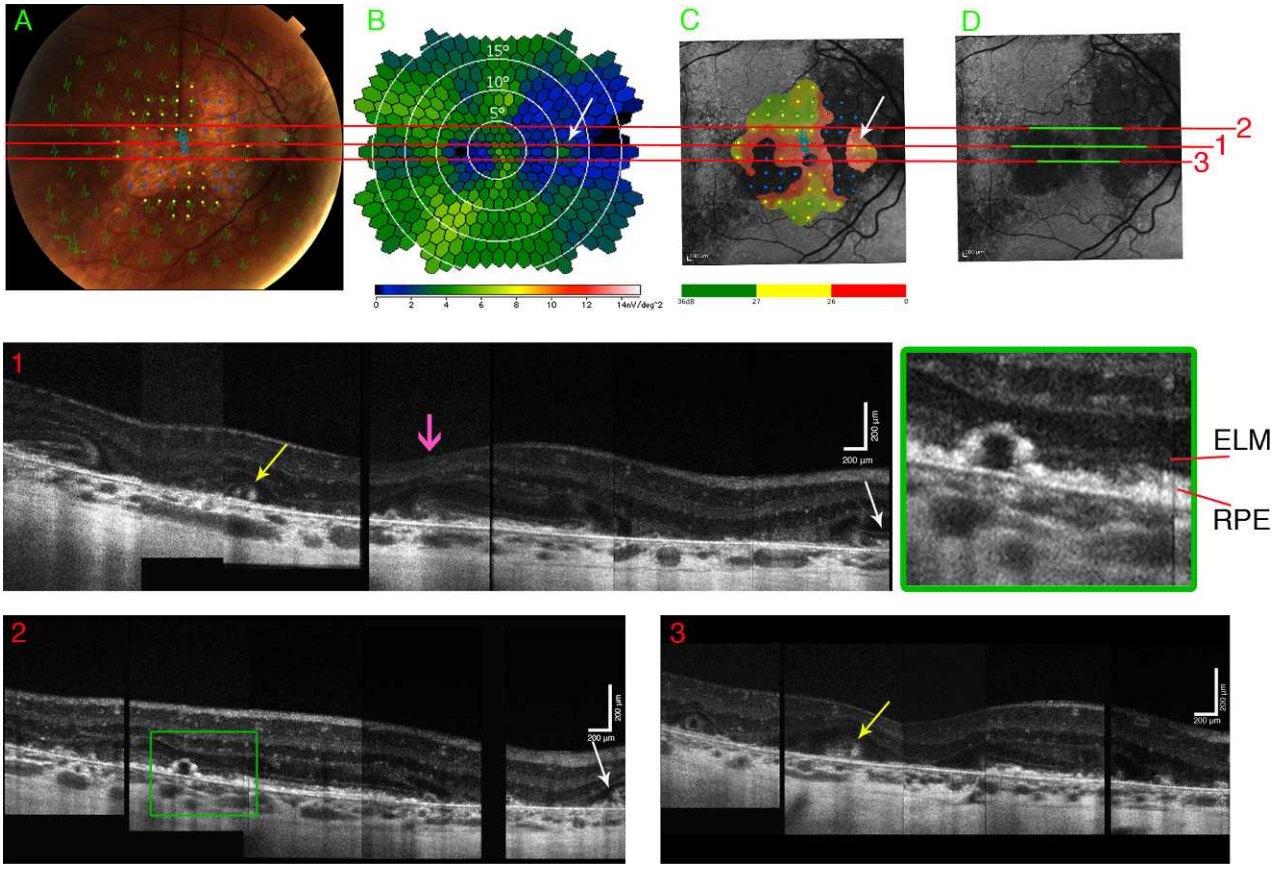

Figure 4. Results from subject GA3. The panel layout is the same as in Figure 1. The *white arrows* in scans 1 and 2 correspond to the *white arrows* in (**B**, **D**) where there is preserved function as measured with photopic mfERGs and mP. The *yellow arrows* in scans 1 and 3 correspond to the hyperautofluorescent strip shown in (**D**). The magnified scan shows a druse with remaining RPE and ELM reflectivity but without IS/OS junction reflectivity.

an autofluorescent strip running through the central atrophic region that can be also seen in B-scans 1 and 3 (yellow arrows; also, note the choroidal hyporeflectance). However, this retinal strip looks disorganized without well-defined outer retinal bands.

The FAF of subject GA4 (Fig. 5) shows areas of atrophy with a leading border of hyperautofluorescence. A small area of the temporal retina still responds to light stimulation when probed with mP. Both tests generally agree with the FAF hypoautofluorescent atrophic area (see also Fig. 7). Photopic mfERGs show that response density is abnormal (>2.5 SD from age-matched normals) in the temporal-superior retina where reticular autofluorescence is evident while it is at the lower limits of normal in the temporal-inferior retina that shows normal autofluorescence. Photopic mfERG implicit time is severely abnormal throughout the whole retinal area tested (>2.5 SD from age-matched normals). Here, it should be noted that the mfERG response density map, shown on Figure 5B, could be misleading. At the center of the hexagonal pattern, there is an area that seems to show electrophysiological activity (white arrow on Fig. 5B). However, CF, FAF, and mfERG traces show that this area is atrophic. This false positive result is due to the way the mfERG response density is calculated. Because the area of the central hexagons is very small, there the ERG signal noise can yield a false response density when divided by a small area (for a more extensive description of this problem, refer to Hood et al.[57(p12)] The central AO-OCT B-scan (1) shows an extensive atrophic lesion with subretinal fibrosis (white arrow). The magenta arrow indicates the PRL that is right at the edge of the atrophy where there is remaining RPE. The two other B-scans show the atrophic area with remaining RPE at the edge of the atrophy. B-scan 3 shows an extension of the retinal scar shown on scan 1 (white arrow). Similarly with other subjects, the IS/OS junction is not reflective close to the border of atrophy where ELM reflectivity is preserved (see magnified B-scans).

Figure 6 shows the grouped photopic mfERG responses for the four GA subjects. Three different groups were formed depending on the retinal condition (GA, peri-GA, non-GA). The central hexagon that corresponds to the fovea was treated separately. The first group was the GA group that corresponded to hexagons stimulating the atrophic lesions. We kept the criterion that at least 50% of the hexagonal area was stimulating atrophic retina. The second group (peri-GA) consists of the hexagons that are adjacent to the first group and therefore adjacent to the atrophy. The third group (non-GA) consisted of all the remaining hexagons. However, because of the size and geometry of the hexagons, peri-GA and non-GA areas were unavoidably grouped in the GA group. The black traces are the age-matched normal responses.

It can be seen from Figure 6 that the foveal hexagon shows lower responses than normal for all subjects. The GA group shows abnormal responses for subjects GA2, GA3, and GA4, but it is normal for subject GA1 due to the retinal extension of the stimuli. The peri-GA group is normal only for subjects GA1 and GA2, while all subjects show normal responses in the non-GA group. The N1P1 amplitude (difference between P1 and N1 amplitude) between the GA subjects and age-matched normals

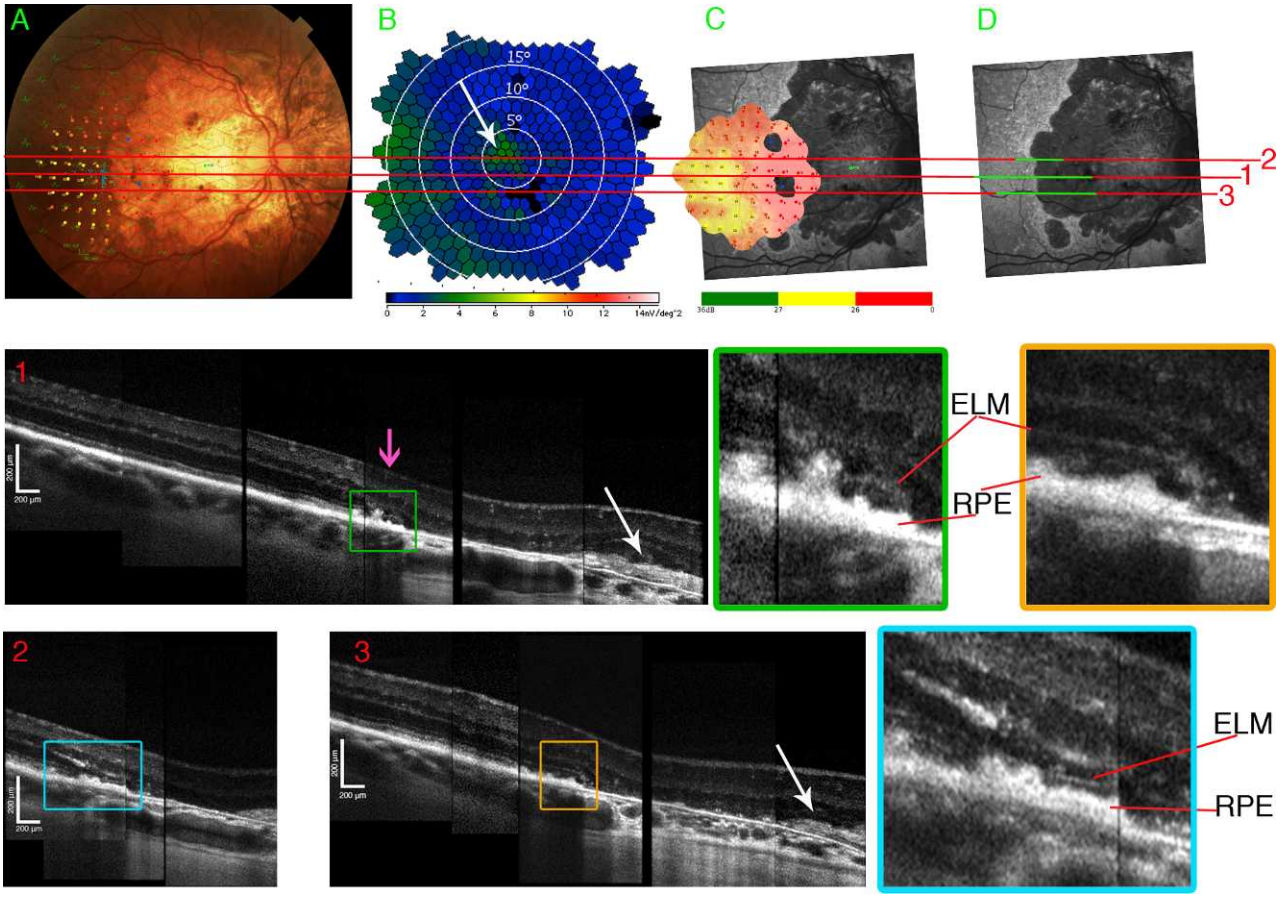

Figure 5. Results from subject GA4. The panel layout is the same as in Figure 1. The *white arrows* on scans 1 and 3 point to the subretinal fibrosis. The magnified scans show the edge of the atrophy where IS/OS junction is not present. The *white arrow* on (**B**) shows the false positive mfERG response density (for an explanation, refer to Results in the text).

for the same four retinal locations as in Figure 6, is plotted in Figure 7. Note that a zero difference means that there is no difference in the N1P1 amplitudes of GA patients and age-matched normal. The fovea shows the largest difference between GA and normals and the largest interindividual variability as shown by the error bars (±1 SD). The N1P1 difference is reduced as the groups move away from the GA and minimized for the non-GA group, as expected.

Figure 8 shows the scotopic mfERG traces for the normal and three GA subjects (GA1–GA3), superimposed on their CF images (subject GA4 was not able to locate the fixation cross under dark-adapted conditions and therefore she did not complete this test). The normal subject (Fig. 8, N1) showed almost uniform responses across his retina, except the central hexagon and hexagons adjacent to it where the responses were lower, following the rod density distribution. Subject GA2 showed responses comparable with normal (<1 SD). Subject GA2 showed no responses throughout his macula (up to 12° eccentricity) while for eccentricities more than 12°, his responses returned to normal. Subject GA3 showed responses comparable to subjects N1 and GA1 in her peripheral retina (>12° eccentricity) while in the atrophic areas, the scotopic mfERG responses were absent or highly reduced.

Discussion

Ultrahigh resolution OCT imaging with adaptive optics was compared with clinical imaging (CF, FAF) and functional eye tests (i.e., mfERGs and mP) on patients with GA. Our aim was to offer new insight in understanding the disease by better visualizing diseased retinae and correlating structural details to functional tests.

OCT and Retinal Function

In three out of four GA patients imaged in this study, we saw that the IS/OS junction lost its reflectivity while still retaining underlying RPE. The ELM and OPL extended up to the GA margin and their endpoint did not correspond to the IS/OS junction's reflectivity. Because of the difficulty of visualizing the outer retinal bands with commercial SD-OCT systems, determining photoreceptor loss was problematic. The functional tests showed that there was still remaining photoreceptor function at the margins of the GA even though IS/OS junction reflectivity was not evident. The clearest example in this category was patient GA1 whose PRL falls within an atrophic area with remaining RPE. The ELM's reflectivity extended within the atrophy without corresponding IS/OS junction reflectivity. However, her PRL in this part of the retina demonstrated some preserved function. The loss of reflectivity might be due to disorganization of the cones and, as a consequence, loss in light coupling or their wave-guide ability. It has been proposed that the IS/OS junction reflectivity, as used historically in the OCT literature, may originate from the mitochondria present in the cone ellipsoids.[52] The authors of this manuscript, as explained in the methods, still think that IS/OS signal originates from changes in optical properties of the

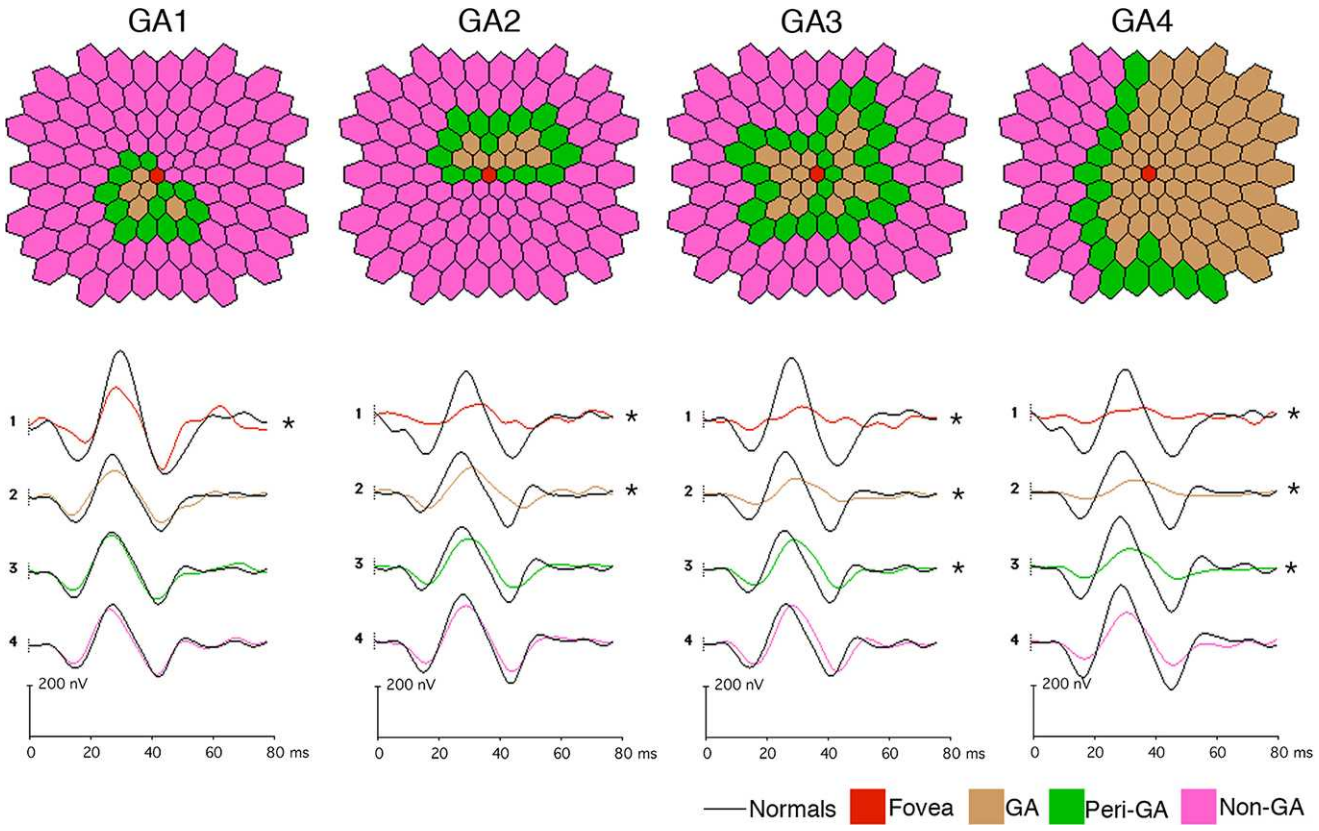

Figure 6. Averaged photopic mfERG responses over different retinal areas. Each *column* corresponds to one GA subject. The central hexagon that corresponds to the fovea is shown ungrouped (*red*). The rest of the hexagons are grouped depending on the retinal area stimulated. The *brown hexagons* correspond to atrophic areas. The *green hexagons* correspond to the area adjacent to the GA (peri-GA group). The *magenta hexagons* correspond to retinal areas that are nonatrophic and nonadjacent to atrophic lesions. The averaged responses are shown *below* the hexagonal pattern and are color-coded similarly to the groups. The *black traces* are the averaged responses of age-matched normals. An *asterisk next* to a *trace* denotes that there is a statistically significant difference from normal.

inner and outer segments as seen by wave-guided photons propagating inside the segments. Thus, it is a reflection from the single junction rather than backscattered signal from extended depth within cone inner segments. However, as the exact location of the reflectivity remains controversial and its origin may be significant for disease diagnosis, more studies need to be performed in the future. Recently, Henle's fibers, which are usually not visible with standard OCT, were revealed by simply displacing the entry position of the beam from the center of the pupil to the periphery.[58,59] We used this approach to image one of the GA patients (GA1, see Fig. 9) and confirmed that indeed there is IS/OS junction reflectivity underneath the ELM (Fig. 9, right panel) which is responsible for functional vision and wasn't visible when positioning the OCT beam in the center of the eye pupil. Hence, attention should be paid to the importance of functional measurements, as a complement to imaging, in order to identify functional retinal areas having an important role in the everyday life of the patient.

OCT and Hypoautofluorescence

As outlined in the introduction, FAF is a useful imaging modality for the identification of the GA margins and quantification of the disease progression using the hypoautofluorescent areas as biomarkers.[15,60,61] Whether a hypoautofluorescent area is truly RPE atrophy is uncertain. Patient GA2's FAF image shows areas of hypoautofluorescence distributed across the macula being larger and more prominent in the superior macula. On an AO-OCT image, these areas appear with hyperreflective calcified drusen that block the OCT light from penetrating deeper to help quantify the amount of remaining RPE. Conversely, the lack of autofluorescence from RPE on an FAF image may be because the lipofuscin either cannot be excited by the short wavelength light or because the RPE autofluorescence cannot penetrate the calcified drusen to reach the detector. In such cases, we can neither conclude nor rule out the possibility that these hypoautofluorescent areas are GA. However, we are able to track the RPE layer and define its boundaries on an AO-OCT image (as in Fig. 3). FAF images, along with CF images, are of great help when it comes to GA grading.[11] However, FAF images should be accompanied with OCT imaging, when possible, to exclude the presence of light blockers that can overestimate the GA area.

Hyperautofluorescence and Retinal Function

Hyperautofluorescent signal on an FAF image is thought to be due to an increase in lipofuscin accumulation in the RPE cells[62] (but see also Theelen et al.,[63] Morgan and Pugh[64] and Rudolf et al.[65]), it is correlated with a decline in visual function measured with mP[44] and whether it has any predictive value on the progression of GA areas is still to be shown.[15,66] In this report, three out of four subjects (GA2, GA3, and GA4) show increased granulated autofluorescence in their peripheral retina. We would expect that their function as measured by mfERGs would be decreased in these areas. However, the mfERG results do not confirm this hypothesis as they appear to be

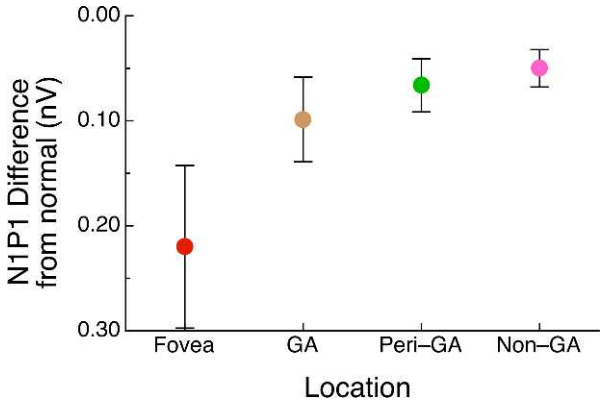

FIGURE 7. Difference of GA patients' averaged mfERG N1P1 responses from age-matched normal mfERGs for the four retinal locations described in Figure 6.

normal for areas away from the GA and peri-GA loci (see Fig. 6). We were unable to confirm the same finding with mP as the testing size is smaller than the mfERGs. It is known that lipofuscin accumulation increases with age and its phototoxic properties gradually affect the RPE apoptotic process.[14] To our knowledge, there is not an established threshold of lipofuscin density (as it could be defined by FAF) after which visual function is affected. The evidence of compromised function due to hyperautofluorescence is sound, but mP, which is used in most of these studies, does not extend beyond a 5° to 10° eccentricity.[44] Here, subjects GA2, GA3, and GA4 show hyperautofluorescence at the peripheral retina beyond 8° eccentricity. The mP is a valuable clinical test for the integrity of the central macula. It would be interesting to extend the microperimetric measurements to higher eccentricities as many patients (especially GA patients) rely on their macular edge for everyday activities.

Photopic and Scotopic mfERGs in GA

Some functional and histopathological studies have reported that the rod-mediated system is more vulnerable than the cone-mediated system to aging, lipofuscin accumulation, and maculopathies.[33,36,67,68] However, other electrophysiological studies showed that cone-mediated mfERGs are equally affected in patients with early age-related macular degeneration when they are monitored over a long period of time.[69] As expected, our photopic and scotopic mfERG results show that there is almost a complete loss of cone- and rod-mediated responses in GA areas. The cone-mediated mfERG response densities are low at the margins of GA and normal beyond the GA margins. The scotopic mfERGs are evident outside the GA margins as subjects GA1 and GA3 show scotopic responses comparable to subject N1, outside the GA areas. Subject GA2, whose macula is affected by multiple drusen, shows compromised scotopic responses across the whole macula, which is in agreement with previously reported findings that rods are more vulnerable than cones in AMD.[33,36] Scotopic mfERGs do not provide a detailed map of the peri-GA and non-GA areas, in the same way as the cone-mediated mfERGs do, because of the large hexagonal size. However, as the results show here, scotopic mfERGs are more sensitive on detecting functional changes in areas where photopic mfERGs appear normal. Hence, an effort on creating scotopic mfERG protocols of higher resolution might favor early detection of rod abnormality as measured with the mfERG technique.

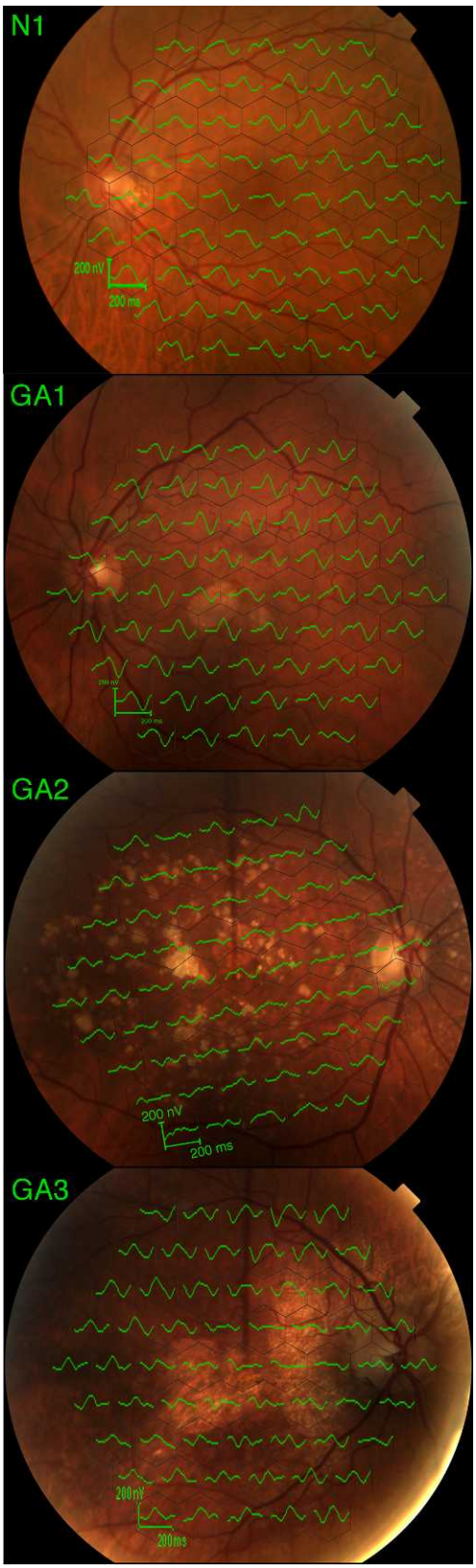

FIGURE 8. The scotopic mfERG responses of the normal and three GA subjects (GA1–3) superimposed on their CF.

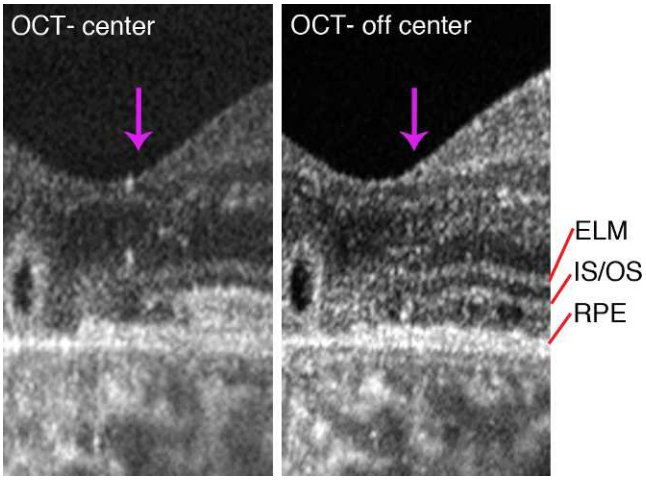

FIGURE 9. OCT B-scans of the same retinal area but different beam entry in the plane of the pupil. The *left scan* was acquired with the entry position of the beam at the center of the pupil while for the *right scan*, the beam was positioned at the pupil's periphery (~1.6 mm from the pupil center). The *magenta arrows* indicate the subject's PRL. Note the IS/OS junction reflectivity underneath the ELM in the *right panel* that is not visible in the *left panel*.

Structure Versus Function or Structure and Function?

The images provided here advance our knowledge of the retinal layers in GA patients and how CF and FAF findings appear with anatomical delineation by AO-OCT technology. We were able to functionally and structurally evaluate retinae of patients with GA and register the various structural and functional mappings of diseased retinae at unprecedented resolution. Retinal structure correlates well between AO-OCT and FAF; however, a few examples of miscategorized structures emphasize the importance of diagnoses based on both modalities. Retinal function correlates between mP and mfERGs without evidence of inconsistency. However, when function is correlated with retinal structure, as detected by imaging modalities such as FAF and OCT, it offers new insights into the interpretation of measured structural changes. The functional tests demonstrate the feasibility of correlating structure with function, even with patients having poor fixation, to monitor for progression of advanced AMD, provided care is taken to register the images based on first determining the PRL. Future applications of multimodal imaging systems may make possible the simultaneous structural and functional testing during a single patient visit.[70,71]

Acknowledgments

The authors thank Erich Sutter for his help on the scotopic mfERGs, Susan Garcia for her efforts on coordinating all the tests with the patients, and Sang Hyuck Lee for Zemax modeling.

Supported by Grant AG 04058 from the National Institute on Aging (JSW); EY 014743 from the National Eye Institute (JSW) and Research to Prevent Blindness. AGC is supported by the Lawrence Scholar Program (LSP) at Lawrence Livermore National Laboratory and this work was performed in part under the auspices of the US Department of Energy under Contract DE-AC52-07NA27344.

Disclosure: **A. Panorgias**, None; **R.J. Zawadzki**, None; **A.G. Capps**, None; **A.A. Hunter**, None; **L.S. Morse**, None; **J.S. Werner**, None

References

1. Blair CJ. Geographic atrophy of the retinal pigment epithelium. A manifestation of senile macular degeneration. *Arch Ophthalmol*. 1975;93:19–25.
2. Bhutto I, Lutty G. Understanding age-related macular degeneration (AMD): relationships between the photoreceptor/retinal pigment epithelium/Bruch's membrane/choriocapillaris complex. *Mol Aspects Med*. 2012;33:295–317.
3. Sarks JP, Sarks SH, Killingsworth MC. Evolution of geographic atrophy of the retinal pigment epithelium. *Eye*. 1988;2:552–577.
4. Green WR, Key SN III. Senile macular degeneration: a histopathologic study. *Trans Am Ophthalmol Soc*. 1977;75:180–254.
5. Sunness JS. Choroidal neovascularisation and atrophy. *Br J Ophthalmol*. 2006;90:398–399.
6. Scholl HP, Fleckenstein M, Fritsche LG, et al. CFH, C3 and ARMS2 are significant risk loci for susceptibility but not for disease progression of geographic atrophy due to AMD. *PloS One*. 2009;4:e7418.
7. Sepp T, Khan JC, Thurlby DA, et al. Complement factor H variant Y402H is a major risk determinant for geographic atrophy and choroidal neovascularization in smokers and nonsmokers. *Invest Ophthalmol Vis Sci*. 2006;47:536–540.
8. Meleth AD, Wong WT, Chew EY. Treatment for atrophic macular degeneration. *Curr Opin Ophthalmol*. 2011;22:190–193.
9. Bearelly S, Chau FY, Koreishi A, Stinnett SS, Izatt JA, Toth CA. Spectral domain optical coherence tomography imaging of geographic atrophy margins. *Ophthalmology*. 2009;116:1762–1769.
10. Fleckenstein M, Charbel, Issa P, Helb HM, et al. High-resolution spectral domain-OCT imaging in geographic atrophy associated with age-related macular degeneration. *Invest Ophthalmol Vis Sci*. 2008;49:4137–4144.
11. Khanifar AA, Lederer DE, Ghodasra JH, et al. Comparison of color fundus photographs and fundus autofluorescence images in measuring geographic atrophy area. *Retina*. 2012;32:1884–1891.
12. Mauschitz MM, Fonseca S, Chang P, et al. Topography of geographic atrophy in age-related macular degeneration. *Invest Ophthalmol Vis Sci*. 2012;53:4932–4939.
13. Holz FG, Bindewald-Wittich A, Fleckenstein M, et al. Progression of geographic atrophy and impact of fundus autofluorescence patterns in age-related macular degeneration. *Am J Ophthalmol*. 2007;143:463–472.
14. Delori FC, Dorey CK, Staurenghi G, Arend O, Goger DG, Weiter JJ. In vivo fluorescence of the ocular fundus exhibits retinal pigment epithelium lipofuscin characteristics. *Invest Ophthalmol Vis Sci*. 1995;36:718–729.
15. Holz FG, Bellmann C, Margaritidis M, Schutt F, Otto TP, Volcker HE. Patterns of increased in vivo fundus autofluorescence in the junctional zone of geographic atrophy of the retinal pigment epithelium associated with age-related macular degeneration. *Graefes Arch Clin Exp Ophthalmol*. 1999;237:145–152.
16. Zawadzki RJ, Jones SM, Olivier SS, et al. Adaptive-optics optical coherence tomography for high-resolution and high-speed 3D retinal in vivo imaging. *Optics Express*. 2005;13:8532–8546.
17. Hammer DX, Iftimia NV, Ferguson RD, et al. Foveal fine structure in retinopathy of prematurity: an adaptive optics Fourier domain optical coherence tomography study. *Invest Ophthalmol Vis Sci*. 2008;49:2061–2070.
18. Werner JS, Keltner JL, Zawadzki RJ, Choi SS. Outer retinal abnormalities associated with inner retinal pathology in nonglaucomatous and glaucomatous optic neuropathies. *Eye*. 2011;25:279–289.

19. Choi SS, Zawadzki RJ, Lim MC, et al. Evidence of outer retinal changes in glaucoma patients as revealed by ultrahigh-resolution in vivo retinal imaging. *Br J Ophthalmol*. 2011; 95:131–141.
20. Hermann B, Fernandez EJ, Unterhuber A, et al. Adaptive-optics ultrahigh-resolution optical coherence tomography. *Opt Lett*. 2004;29:2142–2144.
21. Povazay B, Hofer B, Torti C, et al. Impact of enhanced resolution, speed and penetration on three-dimensional retinal optical coherence tomography. *Opt Express*. 2009;17:4134–4150.
22. Zawadzki RJ, Cense B, Zhang Y, Choi SS, Miller DT, Werner JS. Ultrahigh-resolution optical coherence tomography with monochromatic and chromatic aberration correction. *Opt Express*. 2008;16:8126–8143.
23. Zhang Y, Rha J, Jonnal R, Miller D. Adaptive optics parallel spectral domain optical coherence tomography for imaging the living retina. *Opt Express*. 2005;13:4792–4811.
24. Sunness JS, Ziegler MD, Applegate CA. Issues in quantifying atrophic macular disease using retinal autofluorescence. *Retina*. 2006;26:666–672.
25. Berrow EJ, Bartlett HE, Eperjesi F, Gibson JM. The electroretinogram: a useful tool for evaluating age-related macular disease? *Doc Ophthalmol*. 2010;121:51–62.
26. Gerth C. The role of the ERG in the diagnosis and treatment of age-related macular degeneration. *Doc Ophthalmol*. 2009;118: 63–68.
27. Palmowski AM. Multifocal stimulation techniques in ophthalmology – Current knowledge and perspectives. *Strabismus*. 2003;11:229–237.
28. Sutter EE, Tran D. The field topography of ERG components in man–I. The photopic luminance response. *Vision Res*. 1992; 32:433–446.
29. Chen C, Wu L, Wu D, et al. The local cone and rod system function in early age-related macular degeneration. *Doc Ophthalmol*. 2004;109:1–8.
30. Huang S, Wu D, Jiang F, et al. The multifocal electroretinogram in age-related maculopathies. *Doc Ophthalmol*. 2000;101: 115–124.
31. Li J, Tso MO, Lam TT. Reduced amplitude and delayed latency in foveal response of multifocal electroretinogram in early age related macular degeneration. *Br J Ophthalmol*. 2001;85:287–290.
32. Curcio CA. Photoreceptor topography in ageing and age-related maculopathy. *Eye*. 2001;15:376–383.
33. Curcio CA, Medeiros NE, Millican CL. Photoreceptor loss in age-related macular degeneration. *Invest Ophthalmol Vis Sci*. 1996;37:1236–1249.
34. Jackson GR, McGwin G Jr., Phillips JM, Klein R, Owsley C. Impact of aging and age-related maculopathy on activation of the a-wave of the rod-mediated electroretinogram. *Invest Ophthalmol Vis Sci*. 2004;45:3271–3278.
35. Jackson GR, McGwin G Jr., Phillips JM, Klein R, Owsley C. Impact of aging and age-related maculopathy on inactivation of the a-wave of the rod-mediated electroretinogram. *Vision Res*. 2006;46:1422–1431.
36. Feigl B, Brown B, Lovie-Kitchin J, Swann P. Cone- and rod-mediated multifocal electroretinogram in early age-related maculopathy. *Eye*. 2005;19:431–441.
37. Feigl B, Brown B, Lovie-Kitchin J, Swann P. Monitoring retinal function in early age-related maculopathy: visual performance after 1 year. *Eye*. 2005;19:1169–1177.
38. Feigl B, Brown B, Lovie-Kitchin J, Swann P. The rod-mediated multifocal electroretinogram in aging and in early age-related maculopathy. *Curr Eye Res*. 2006;31:635–644.
39. Gerth C, Hauser D, Delahunt PB, Morse LS, Werner JS. Assessment of multifocal electroretinogram abnormalities and their relation to morphologic characteristics in patients with large drusen. *Arch Ophthalmol-Chic*. 2003;121:1404–1414.
40. Parisi V, Perillo L, Tedeschi M, et al. Macular function in eyes with early age-related macular degeneration with or without contralateral late age-related macular degeneration. *Retina*. 2007;27:879–890.
41. Parravano M, Oddone F, Tedeschi M, et al. Retinal functional changes measured by microperimetry in neovascular age-related macular degeneration patients treated with ranibizumab. *Retina*. 2009;29:329–334.
42. Sunness JS, Schuchard RA, Shen N, Rubin GS, Dagnelie G, Haselwood DM. Landmark-driven fundus perimetry using the scanning laser ophthalmoscope. *Invest Ophthalmol Vis Sci*. 1995;36:1863–1874.
43. Holopigian K, Seiple W, Greenstein V, Kim D, Carr RE. Relative effects of aging and age-related macular degeneration on peripheral visual function. *Optom Vis Sci*. 1997;74:152–159.
44. Midena E, Vujosevic S, Convento E, Manfre A, Cavarzeran F, Pilotto E. Microperimetry and fundus autofluorescence in patients with early age-related macular degeneration. *Br J Ophthalmol*. 2007;91:1499–1503.
45. Meleth AD, Mettu P, Agron E, et al. Changes in retinal sensitivity in geographic atrophy progression as measured by microperimetry. *Invest Ophthalmol Vis Sci*. 2011;52:1119–1126.
46. Sunness JS, Johnson MA, Massof RW, Marcus S. Retinal sensitivity over drusen and nondrusen areas. A study using fundus perimetry. *Arch Ophthalmol-Chic*. 1988;106:1081–1084.
47. Hood DC, Wladis EJ, Shady S, Holopigian K, Li J, Seiple W. Multifocal rod electroretinograms. *Invest Ophthalmol Vis Sci*. 1998;39:1152–1162.
48. Zawadzki RJ, Choi SS, Fuller AR, Evans JW, Hamann B, Werner JS. Cellular resolution volumetric in vivo retinal imaging with adaptive optics-optical coherence tomography. *Opt Express*. 2009;17:4084–4094.
49. *ImageJ* [computer program]. Bethesda, MD: U.S. National Institutes of Health; 1999–2012.
50. Thévenaz P, Ruttimann, UE, Unser, M. A pyramid approach to subpixel registration based on intensity. *IEEE T Image Process*. 1998;7:27–41.
51. Lu RW, Curcio CA, Zhang Y, et al. Investigation of the hyperreflective inner/outer segment band in optical coherence tomography of living frog retina. *J Biomed Opt*. 2012;17: 060504.
52. Spaide RF, Curcio CA. Anatomical correlates to the bands seen in the outer retina by optical coherence tomography: literature review and model. *Retina*. 2011;31:1609–1619.
53. Marcuse D. Loss analysis of single-mode fiber splices. *AT&T Tech J*. 1977;56:703–718.
54. Giallorenzi TG, Bucaro JA, Dandridge A, et al. Optical fiber sensor technology. *IEEE J Quantum Elect*. 1982;18:626–665.
55. Gao W, Cense B, Zhang Y, Jonnal RS, Miller DT. Measuring retinal contributions to the optical Stiles-Crawford effect with optical coherence tomography. *Opt Express*. 2008;16:6486–6501.
56. Mones J, Biarnes M, Trindade F. Hyporeflective wedge-shaped band in geographic atrophy secondary to age-related macular degeneration: an underreported finding. *Ophthalmology*. 2012;119:1412–1419.
57. Hood DC, Bach M, Brigell M, et al. ISCEV standard for clinical multifocal electroretinography (mfERG) (2011 edition). *Doc Ophthalmol*. 2012;124:1–13.
58. Lujan BJ, Roorda A, Knighton RW, Carroll J. Revealing Henle's fiber layer using spectral domain optical voherence tomography. *Invest Ophthalmol Vis Sci*. 2011;52:1486–1492.

Investigative Ophthalmology & Visual Science

59. Otani T, Yamaguchi Y, Kishi S. Improved visualization of Henle fiber layer by changing the measurement beam angle on optical coherence tomography. *Retina*. 2011;31:497–501.
60. Delori FC, Fleckner MR, Goger DG, Weiter JJ, Dorey CK. Autofluorescence distribution associated with drusen in age-related macular degeneration. *Invest Ophthalmol Vis Sci*. 2000;41:496–504.
61. Kennedy CJ, Rakoczy PE, Constable IJ. Lipofuscin of the retinal pigment epithelium: a review. *Eye*. 1995;9(pt 6);763–771.
62. von Ruckmann A, Fitzke FW, Bird AC. Fundus autofluorescence in age-related macular disease imaged with a laser scanning ophthalmoscope. *Invest Ophthalmol Vis Sci*. 1997; 38:478–486.
63. Theelen T, Berendschot TT, Boon CJ, Hoyng CB, Klevering BJ. Analysis of visual pigment by fundus autofluorescence. *Exp Eye Res*. 2008;86:296–304.
64. Morgan JI, Pugh EN Jr. Scanning laser ophthalmoscope measurement of local fundus reflectance and autofluorescence changes arising from rhodopsin bleaching and regeneration. *Invest Ophthalmol Vis Sci*. 2013;54:2048–2059.
65. Rudolf M, Vogt SD, Curcio CA, et al. Histologic basis of variations in retinal pigment epithelium autofluorescence in eyes with geographic atrophy. *Ophthalmology*. 2013;120:821–828.
66. Hwang JC, Chan JW, Chang S, Smith RT. Predictive value of fundus autofluorescence for development of geographic atrophy in age-related macular degeneration. *Invest Ophthalmol Vis Sci*. 2006;47:2655–2661.
67. Owsley C, Jackson GR, Cideciyan AV, et al. Psychophysical evidence for rod vulnerability in age-related macular degeneration. *Invest Ophthalmol Vis Sci*. 2000;41:267–273.
68. Scholl HP, Bellmann C, Dandekar SS, Bird AC, Fitzke FW. Photopic and scotopic fine matrix mapping of retinal areas of increased fundus autofluorescence in patients with age-related maculopathy. *Invest Ophthalmol Vis Sci*. 2004;45:574–583.
69. Gerth C, Delahunt PB, Alam S, Morse LS, Werner JS. Cone-mediated multifocal electroretinogram in age-related macular degeneration: progression over a long-term follow-up. *Arch Ophthalmol*. 2006;124:345–352.
70. Hammer DX, Ferguson RD, Mujat M, et al. Multimodal adaptive optics retinal imager: design and performance. *JOSA A*. 2012; 29:2598–2607.
71. Zawadzki RJ, Jones SM, Pilli S, et al. Integrated adaptive optics optical coherence tomography and adaptive optics scanning laser ophthalmoscope system for simultaneous cellular resolution in vivo retinal imaging. *Biomed Opt Express*. 2011;2: 1674–1686.

Investigative Ophthalmology & Visual Science